Supporting information for

Interfacial Engineering of Cobalt Nitrides and Mesoporous Nitrogen-doped Carbon: Towards Efficient Overall Water Splitting Activity with Enhanced Charge Transfer Efficiency

Wenyu Yuan,[ab+*] Shiyao Wang,[c+] Yiyuan Ma,[a+] Yu Qiu,[d] Yurong An,[c] Laifei Cheng[a]

[a] Science and Technology on Thermostructural Composite Materials Laboratory, Northwestern Polytechnical University, Xi'an 710072, China.

[b] Global Research Center for Environment and Energy Based on Nanomaterials Science, National Institute for Materials Science (NIMS), Tsukuba 305-0044, Japan

[c] State Key Laboratory of Solidification Processing, Northwestern Polytechnical University, Xi'an 710072, China

[d] Key Lab of Synthetic and Natural Functional Molecule Chemistry of Ministry of Education, College of Chemistry and Materials Science, Northwest University, Xi' an 710069, China

[+] these authors contributed equally to this work

Corresponding author

*Email: YUAN.Wenyu@nims.go.jp

This PDF file includes:

Experiential Details

Figure S1 to S23

Table S1 to S3

References 1-32

Experimental Details

Chemicals:, P123 and Nafion solution (5 wt.%) were purchased from Sigma-Aldrich. Tannin (AR), $Co(OAc)_2$ $4H_2O$ (AR),ethanol (AR), and KOH (AR) were purchased from Aladdin Co. (China). Commerical Pt/C (20 wt.%) was purchased from JM corporation. Commerical RuO_2 was purchased from Premetek company. The deionized water was used in all experiments.

Synthesis of Co₄N@NC: Typically, tannin (1.2 g) and P123 (0.6 g) were mixed in a screw-capped stainless steel reactor (diameter: 4.5 cm, height: 5.5 cm along with nine ball bearings (3×diameter 1.2 cm; 3×diameter 0.7 cm; 3×diameter 0.5 cm). The reactor was placed in a high-speed vibrating ball miller (300 rounds min^{-1}) and the mixtures were ball milled for 1 h. Then, 0.1 g of $Co(OAc)_2$ $4H_2O$ was added into the reactor for ball milling in another 1 h. The resulting gel-like products were washed with deionized H_2O and ethanol, followed by drying at room temperature overnight. Thus the Co-organic precursors was obtained. Then, the obtained precursors were transfered into a quartz tube, and heating under a temperature of (600, 700, 800 °C) for 1 h with a heating rate of 5 °C/s under an atmosphere of NH_3. After naturally cooled down, the Co_4N@NC was obtained, and was denoted as "Co₄N@NC-600", "Co₄N@NC-700", and "Co₄N@NC-800", respectively. The Co₄N@NC through total manuscript is Co₄N@NC-700. The bare Co_4N without NC can be synthesized via the calcination of Co-organic precursos under a temperature of 600 °C in air atmosphere to eliminate carbon, following by the nitridation under 700 °C for 1 h under NH_3 atmosphere. The NC was obtained via similar process without the adding of

Co(OAc)$_2$ 4H$_2$O. The ratio of Co$_4$N in Co$_4$N@NC (R_{Co4N}) can be also calculated via the following equation:

$$R_{Co_4N}(at.\%) = \frac{(m_{Co_4N/NC} - m_{NC})/M_{Co_4N}}{(m_{Co_4N/NC} - m_{NC})/M_{Co_4N} + m_{NC}/M_{NC}} \times 100\% \qquad (1)$$

The R_{Co_4N} in Co$_4$N@NC obtained via above typical process was 1.5 at. %.

Characterizaiton: Powder X-ray diffraction (XRD) patterns were obtained from powders directly with Bruker D8 ADVANCE X-ray diffractometer equipped with Cu Kα radiation. The scanning electron microscopy (SEM, S4700, Hitachi, Japan) equipped with an energy dispersive X-ray spectrometer (EDS) was used to observb the morphologies of Co$_4$N@NC catalysts. Transmission electron microscope (TEM, JEOL-2100) was used to investigate the structure. The elemental composition and chemical bonds were measured via a photoelectron spectroscopy (XPS) (PHI 5400, PE, USA). The SSA were tested by N$_2$ adsorption instrument (Micromeritics ASPA 2460, the United States) using Brunauer–Emmett–Teller (BET) method at 77 K. The pore size distributiton was calculted via using NLDFT method. Raman spectra were obtained from Renishaw Ramascope (Confocal Raman Microscope, Renishaw, Gloucester-shire, U.K.) equipped with a He–Ne laser (λ = 532 nm). The generated H$_2$ and O$_2$ gases were quantified by gas chromatograph (GC, BF3420A, Beijing Beifen-Ruili Analytical Instrument, China).

Electrochemical tests: The HER and OER performance were studied by a typical three-electrode system consisting of a working electrode, a graphite rod counter electrode, and a Ag/AgCl (3.0 M KCl) reference electrode on a CHI 660E electrochemical workstation (Chenhua, Shanghai, China). A glass carbon working

electrode with a diameter of 3 mm was fabricated by the drop-casting the catalyst ink. Typically, 5 mg of catalyst and 100 μL of 5 wt% Nafion solution were dispersed in 900 μL ethanol by 20 min sonication to form a homogeneous ink. After that, 4.3 μL of the above obtained ink (containing ~21.5 μg of catalyst) was coated on the glass carbon electrode (the loading mass: ~ 0.285 mg cm^{-2}). After drying at room temperature, the working electrode was obtained. The Ag/AgCl reference electrode was calibrated with respect to a reversible hydrogen electrode (RHE) by the equation (1):

$$E_{RHE} = E_{Ag/AgCl} + 0.21 + 0.059 pH. \qquad (2)$$

Linear sweep voltammetry (LSV) were carried out in 1 M KOH at a scan rate of 5 mV s^{-1}. Tafel plots are fitted to the Tafel equation:

$$\eta = b \log j + a \qquad (3)$$

where η is the overpotential, b is the Tafel slope, j is the current density and a is the Tafel intercept relative to the exchange current density j_0. Electrochemical impedance spectroscopy (EIS) analysis was tested in the frequency range of 100 kHz to 0.1 Hz under the potential of 100 mV. The electrochemically active surface area (ECSA) was measured by the double layer capacitance (C_{dl}) in a non-faradaic potential range of 0.1 to 0.2 V at different scan rates of 20, 40, 60, 80, 100, and 120 mV·s^{-1}. The ECSA was calculated by the following equation:

$$ECSA = C_{dl}/C_s \qquad (4)$$

Where Cs is the specific capacitance. The durability tests for both HER and OER were carried out at a static potential (corresponding to a relative low current density of

~15 mA cm^{-2}) for 72 h in 1 M KOH with a Hg/HgO reference electrode.

EQCM measurements: EQCM measurements were carried out with a QCM analyzer (QCS-922, Seiko EG&GCo., Ltd.) in 1 M KOH solution. The working electrode for EQCM is via drop-casting of above catalyst ink (13.4 μL) on the gold thin films (*d*=5.3 mm). The mass loading for Co$_4$N is ~0.285 mg cm^{-2}, and the mass loading for Co$_4$N@NC is ~1.14 mg cm^{-2} to ensure that the mass of Co$_4$N on the two electrodes were equal (m$_{Co4N}$ in bare Co$_4$N = m$_{Co4N}$ in Co$_4$N@NC). The counter electrode and reference electrode are graphite rod, and Ag/AgCl, respectively. The overpotential window for HER is -0.3-0 V, while that for OER is 0-0.5 V. The frequency changes were real-time recorded along with the LSV curves. The Sauerbrey equation can be drawn below:[1]

$$\Delta f = -\frac{2f_s^2}{A\sqrt{\mu_q \rho_q}}\Delta m \quad (5)$$

Where f_s=8.96×106 s^{-1}, N is the number for electron transfer, A is the area of working electrode, μ_q=2.947×10^{13} g m-1 s^{-2}, ρ_q=2.648×10^6 g m^{-3}, respectively.[2]

Calculations of TOF: TOF was calculated by a previous method,[3] according to the following formula:

$$TOF = \frac{\text{Total hydrogen (or oxygen) turnovers/cm}^2}{\text{Active sites/cm}^2} \quad (6)$$

$$\text{Hydrogen (or oxygen) turnovers} = (j \times N_A)/(n \times F) = \frac{j \times 6.022 \times 10^{23}}{n \times 96485.3 \times 1000} \quad (7)$$
$$= j \times 6.24 \times 10^{15}/n$$

Where n is the number of electrons, for HER, n=2, for OER, n=4.

The TOF was calculated on Co$_4$N active materials. Therefore, the number of

active sites can be calculated as:

$$\text{Number of active sites} = \text{ratio of active material} \times \text{mass loading} \times \frac{1}{M_{\text{active materials}}} \times 6.022 \times 10^{20} \text{ sites mmol}^{-1} \quad (8)$$

$$= 1.72 \times 10^{17} \text{ sites cm}^{-2}$$

Finally, the TOF can be calculated as:

$$\text{TOF} = \frac{j \times 6.24 \times 10^{15} / n}{1.72 \times 10^{17}} \text{ (s}^{-1}) = 0.0363 \times \frac{j}{n} \text{ (s}^{-1}) \quad (9)$$

DFT calculations: Spin-polarized density functional theory (DFT) calculations were performed using Quantum-ESPRESSO package as implemented in PWscf code.[4] The projector augmented wave (PAW) pseudopotentials were used to describe the interactions between valence electrons and ionic cores.[5] The Perdew-Burke-Ernzerhof (PBE) form of the generalized gradient approximation (GGA) was employed to describe electronic exchange and correlation. [6] We used 50 and 500 Ry cutoffs for the Kinetic energy of the plane-wave basis and charge density, respectively.

To model the $Co_4N@NC$ nanohybrids, a NC nanosheet adsorbed on Co-terminated Co_4N slab with exposed (111) surface was used, resulting in the model with the lowest lattice mismatch for following calculation. The lattice mismatch between NC nanosheet and Co_4N slab is about 5.2%. The supercell consists of 2×2 unit cells for Co_4N slab and 4×4 unit cells for N-doped graphene. A vacuum region of 18 Å was applied in the vertical direction. For $Co_4N@NC$ model, the atoms of four bottom layers of Co_4N slab were fixed at bulk positions while the atoms of four top layers of Co_4N slab and of NC nanosheet were fully relaxed until the maximum force

on a single atom was smaller than 0.05 eV/Å. The Brillouin zone was sampled by 3 ×

3 × 1 uniform k point mesh.[7] The dipole correction is used to remove the effect of

the artificial electric field created by the slab images.[8]

For hydrogen evolution reaction (HER), the reaction Gibbs free energy (ΔG_H) of

H atoms adsorbed to catalysts is calculated by:

$$\Delta G_H = \Delta E_H + \Delta E_{ZPE} - T\Delta S_H \quad (10)$$

where ΔE_H, ΔE_{ZPE}, and ΔS_H are the adsorption energy of hydrogen, the zero-point

energy difference between the adsorbed hydrogen and hydrogen in gas phase, and the

entropy difference between adsorbed state and gas phase. The entropy of atomic

hydrogen can be taken as $\Delta S_H = -S_{H2}/2$, where S_{H2} is the entropy of molecule

hydrogen in gas phase. In standard conditions, ΔE_{ZPE}- $T\Delta S_H$ is about 0.24 eV, hence

ΔG_H can be calculated by $\Delta E_H + 0.24$.

The oxygen evolution reaction (OER) follows four elementary steps. Under

electrode potential $U = 0$ V, the reaction Gibbs free energy ΔG for each step can be

calculated by:

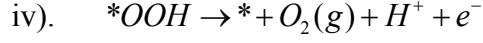i). $H_2O(l) + * \rightarrow *OH + H^+ + e^-$
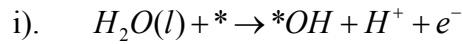
$$\begin{aligned}
\Delta G_1 &= \mu_{*OH} + \mu_{H^+} + \mu_{e^-} - \mu_{H_2O} - \mu_* \\
&= \Delta E_{OH} + \Delta E_{ZPE(OH)} - T\Delta S_{OH} + G_{solv(*OH)} \qquad (11) \\
&= \Delta E_{OH} + 0.1 = \Delta G_{OH}
\end{aligned}$$

ii). $*OH \rightarrow *O + H^+ + e^-$
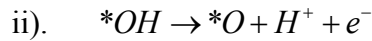
$$\begin{aligned}
\Delta G_2 &= \mu_{*O} + \mu_{H^+} + \mu_{e^-} - \mu_{*OH} \\
&= [\Delta E_O + \Delta E_{ZPE(O)} - T\Delta S_O + G_{solv(*O)}] - [\Delta E_{OH} + \Delta E_{ZPE(OH)} - T\Delta S_{OH} + G_{solv(*OH)}] \quad (12) \\
&= \Delta E_O - \Delta E_{OH} - 0.06 = \Delta G_O - \Delta G_{OH}
\end{aligned}$$

iii). $*O + H_2O(l) \rightarrow *OOH + H^+ + e^-$
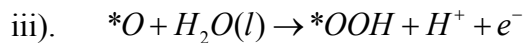
$$\Delta G_3 = \mu_{*OOH} + \mu_{H^+} + \mu_{e^-} - \mu_{H_2O} - \mu_{*O} =$$
$$= [\Delta E_{OOH} + \Delta E_{ZPE(OOH)} - T\Delta S_{OOH} + G_{solv(*OOH)}] - [\Delta E_O + \Delta E_{ZPE(O)} - T\Delta S_O + G_{solv(*O)}] \quad (13)$$
$$= \Delta E_{OOH} - \Delta E_O + 0.06 = \Delta G_{OOH} - \Delta G_O$$

iv). $*OOH \rightarrow * + O_2(g) + H^+ + e^-$

$$\Delta G_1 = \mu_* + \mu_{*O_2} + \mu_{H^+} - \mu_{e^-} - \mu_{OOH}$$
$$= 4.92 - [\Delta E_{OOH} + \Delta E_{ZPE(OOH)} - T\Delta S_{OOH} + G_{solv(*OOH)}] \quad (14)$$
$$= 4.89 - \Delta E_{OOH} = 4.92 - \Delta G_{OOH}$$

Where the ΔE, ΔE_{ZPE}, $T\Delta S$, and G_{solv} are the adsorption energy of molecule, the zero point energy, entropy corrections, and solvation energies corrections to gas or liquid phase molecules and adsorbed species, which are directly taken from Ref [9].

Finally, the theoretical overpotential η, which is determined by the potential limiting step:

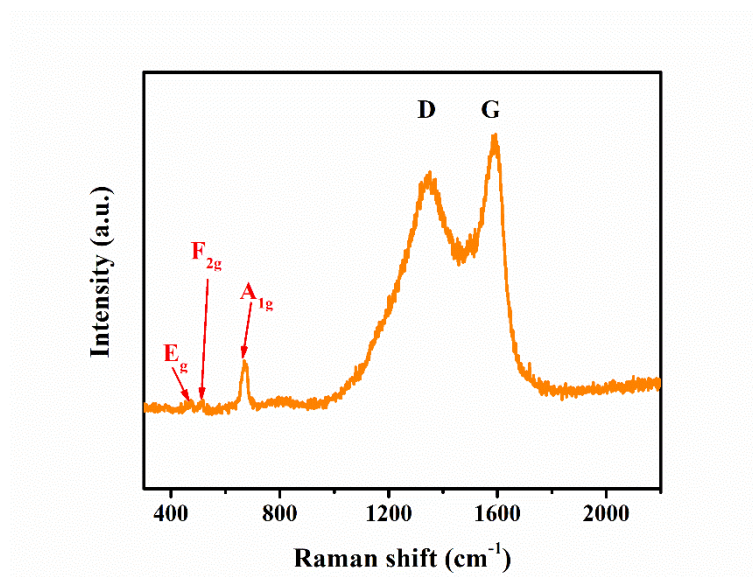$$\eta = \max[\Delta G_1, \Delta G_2, \Delta G_3, \Delta G_4] / e - 1.23[V] \quad (15)$$
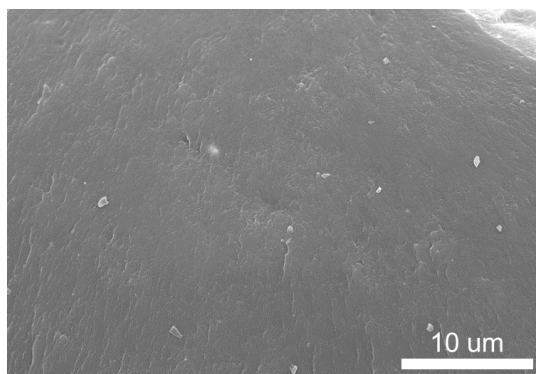
Figure S1. The Raman spectra of $Co_4N@NC$

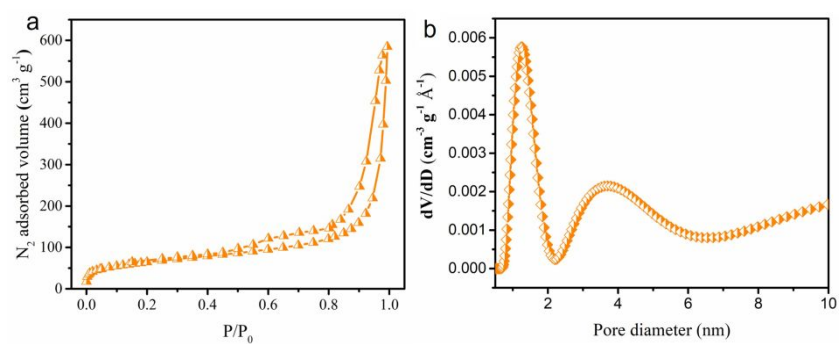Figure S2.The SEM image of precursor after self-assembly

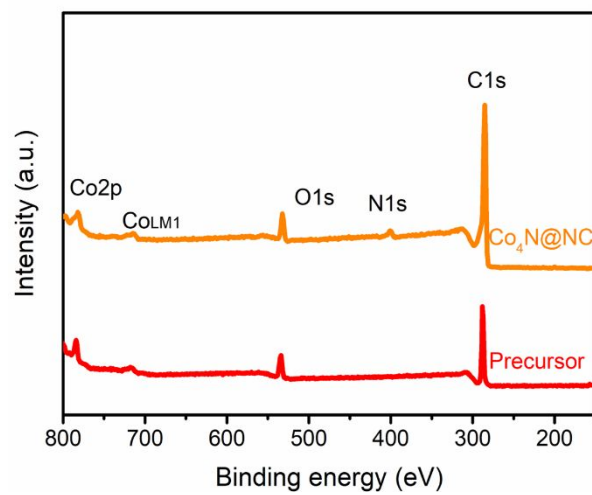Figure S3. N_2 adsorption-desorption curve (a) and the corresponding PSD (b) of $Co_4N@NC$.

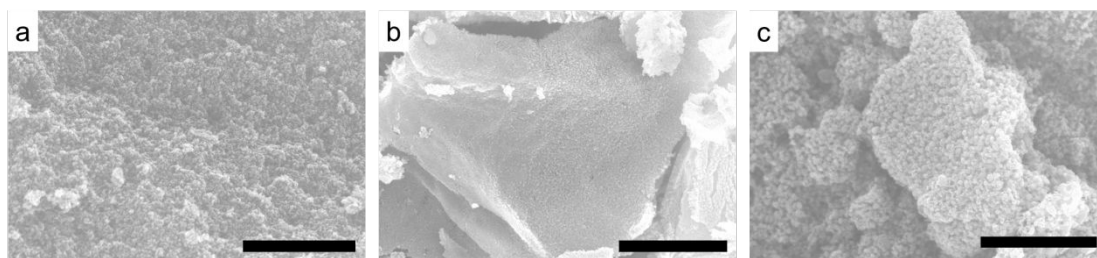Figure S4. The XPS survey spectra of $Co_4N@NC$ and precursor.

Figure S5. (a-c) The SEM images of Co$_4$N@NC-600, Co$_4$N@NC-700, and Co$_4$N@NC-800. The bars are 2 μm.
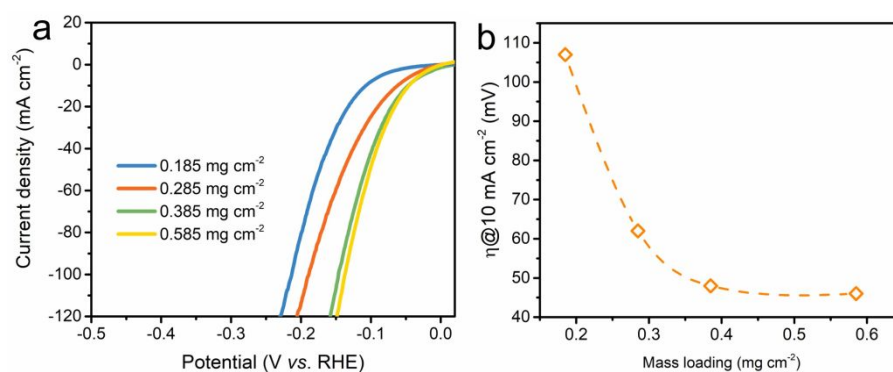
Figure S6. The LSV profiles (a) and the corresponding overpotential@10 mA cm^{-2} (b) of Co4N@NC-700 with different mass loading on GC electrodes.
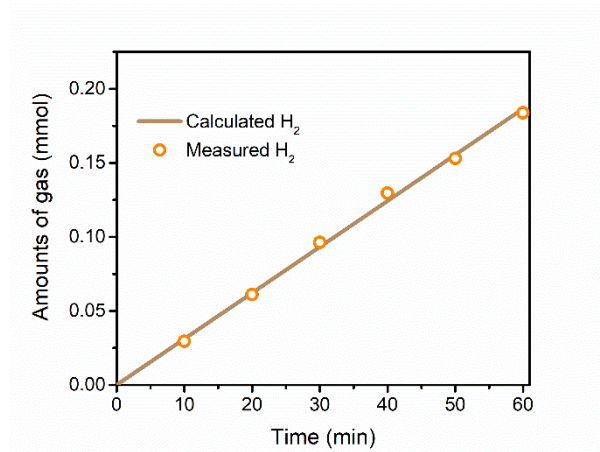
Figure S7. The hydrogen evolution of Co$_4$N@NC at the current density of 10 mA cm^{-2} for 60 min

Table S1. The HER performance of Co$_4$N@NC and other previous reported state-of-art non-precious metal-based catalysts

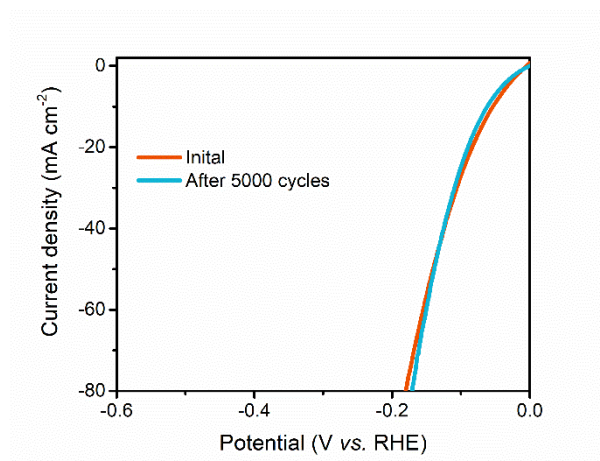| Catalysts	Mass loading (mg cm^{-2})	Media	η@10mA cm^{-2} (mV)	Tafel slopes (mV dec^{-1})	Ref.
Co$_4$N@NC	~0.285	1M KOH	62	37	This work
Ni$_3$FeN-NPs	0.35	1M KOH	158	42	[10]
Co$_3$N	Not given	1M KOH	230	101.6	[11]
Co$_3$O$_4$–Co$_4$N	~2.6	1M KOH	90	57.8	[12]
Co$_{5.47}$N@NC	0.45	1M KOH	149	86	[13]
CoN@VON	2	1M KOH	118	73.6	[14]
CoN@CC	Not given	1M KOH	97	93.9	[15]
FeOOH@Co$_4$N	~2	1M KOH	138	34	[16]
CoO-Co$_4$N	Not given	1M PBS	145	80	[17]
Co(OH)$_2$@Ni	~7.5	1M KOH	96	104	[18]
CoP/rGO	~0.28	1M KOH	150	38	[19]
FeS$_2$/CoS$_2$	~0.2	1M KOH	78.2	44	[20]
CoS$_2$@CC	~1.2	1M KOH	193	88	[21]
Co/N-G	~0.285	0.5M H$_2$SO$_4$	147	82	[22]
N,S-CNT	Not given	1M KOH	~450	133	[23]
Co,N-C	~0.41	0.1M KOH	220	81	[24]
N.F-G	2.55	1M KOH	330	109	[25]
CoP@B,N-C	0.4	1M KOH	215	52	[26]

Figure S8. The LSV polarization curves before and after 5000 cycles.
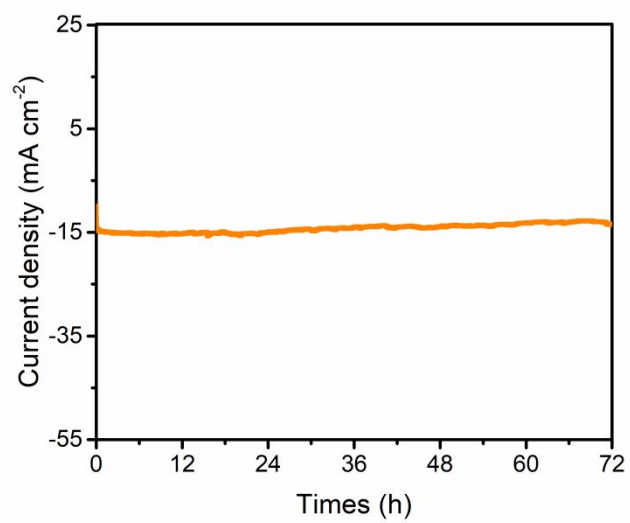
Figure S9. The i-t curves of $Co_4N@NC-700$ under a potential of -78 mV vs. RHE for 72 h.
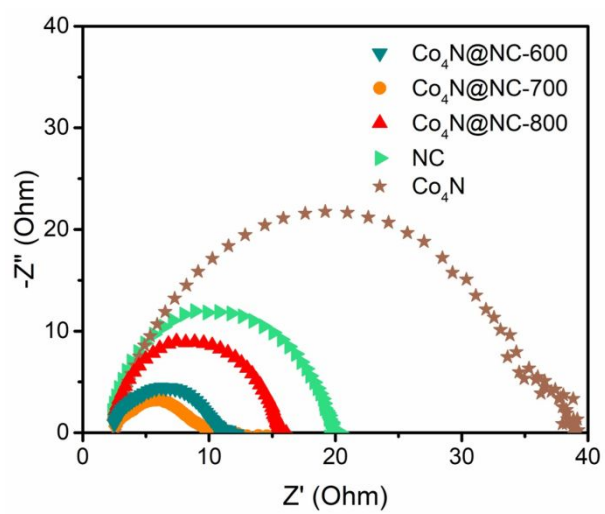
Figure S10. The Nyquist plots of $Co_4N@NC$-600, $Co_4N@NC$-700, $Co_4N@NC$-800, Co_4N, and NC catalysts under a potential of -0.1 V vs. RHE.
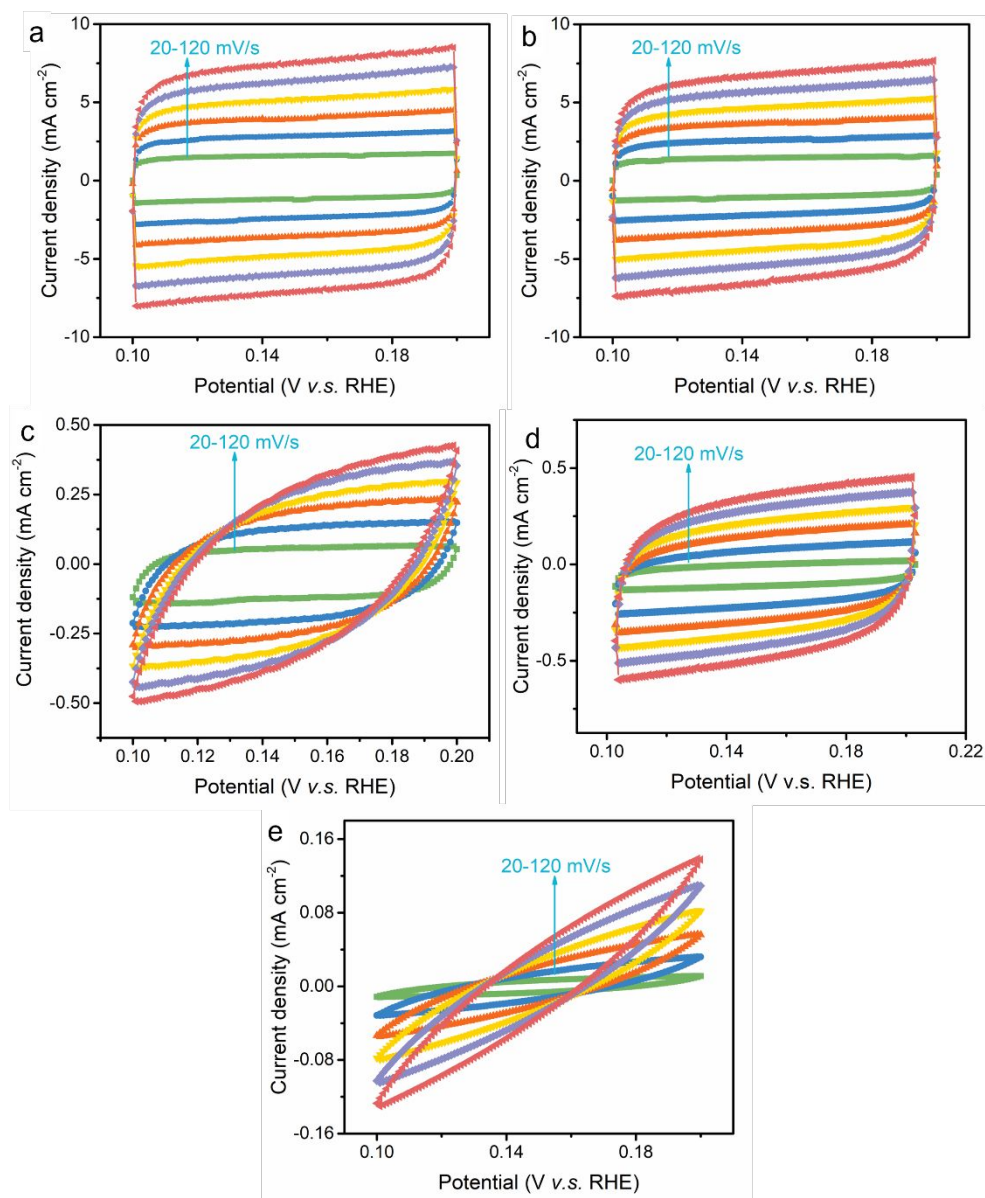
Figure S11. The CV of Co$_4$N@NC-700 (a), Co$_4$N@NC-600 (b), Co$_4$N@NC-800 (c), NC (d), and Co$_4$N (e) at a potential of 0.1-0.2 V v.s. RHE.
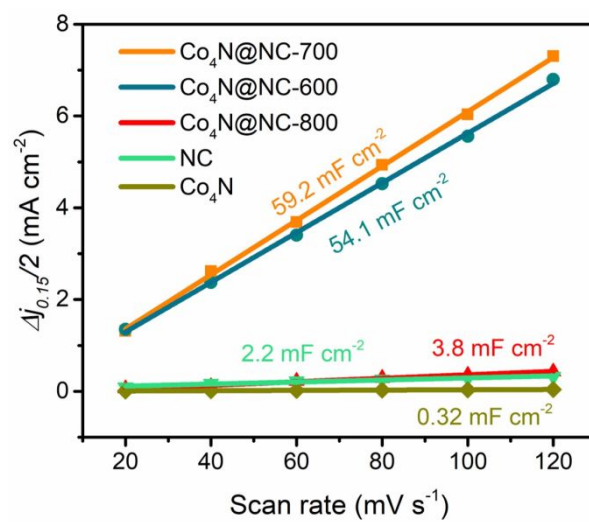
Figure S12. ECSA of Co$_4$N@NC-600, Co$_4$N@NC-700, Co$_4$N@NC-800, Co$_4$N, and NC catalysts
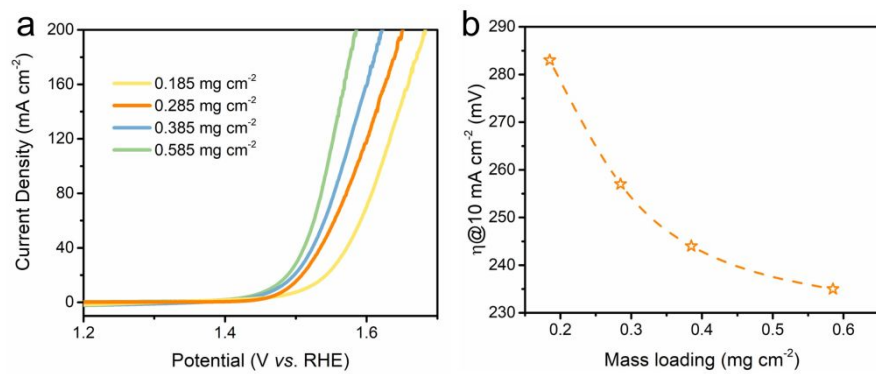
Figure S13. The LSV profiles (a) and the corresponding overpotential@10 mA cm^{-2} (b) of Co$_4$N@NC-700 with different mass loading on GC electrodes for OER.
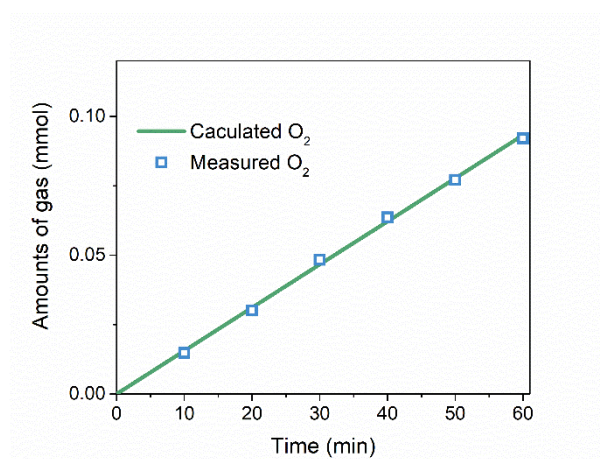
Figure S14. The measured O_2 amounts of $Co_4N@NC$ at the current density of 10 mA cm^{-2} for 60 min.

Table S2. The OER performance of $Co_4N@NC$ and other previous reported state-of-art non-precious metal-based catalysts

| Catalysts	Mass loading (mg cm^{-2})	Media	η@10mA cm^{-2} (mV)	Tafel slopes (mV dec^{-1})	Ref.
$Co_4N@NC$	0.285	1M KOH	261	58	This work
Ni_3FeN-NPs	0.35	1M KOH	280	46	[10]
$FeCo@Co_4N$	0.3	1M KOH	280	40	[27]
Co_4N/CNW/ CC	0.2	1M KOH	310	81	[28]
Co_3N	Not given	1M KOH	330	70	[11]
CoN	Not given	1M KOH	290	70	[29]
$Co_xN@CoP@C$	1	0.1 M KOH	390	78	[30]
$Co_{5.47}N$ @NC	0.45	1M KOH	248	72	[13]
CoN@VON	2	1M KOH	263	64.1	[14]
CoN@CC	Not given	1M KOH	251	75.4	[15]
$FeOOH@Co_4N$	~2	1M KOH	254	84	[16]
CoO-Co_4N	Not given	1M PBS	398	83	[17]
$Co(OH)_2@Ni$	~7.5	1M KOH	300	70.1	[18]
CoOOH	0.15	1M KOH	300	38	[31]
CoP/rGO	~0.28	1M KOH	340	66	[19]
Co/N-C	~0.2	1M KOH	350	79	[32]
$CoS_2@CC$	~1.2	1M KOH	276	81	[21]
N,S-CNT	Not given	1M KOH	360	56	[23]
Co,N-C	~0.41	0.1M KOH	360	83.3	[24]
N,F-G	2.55	1M KOH	340	78	[25]
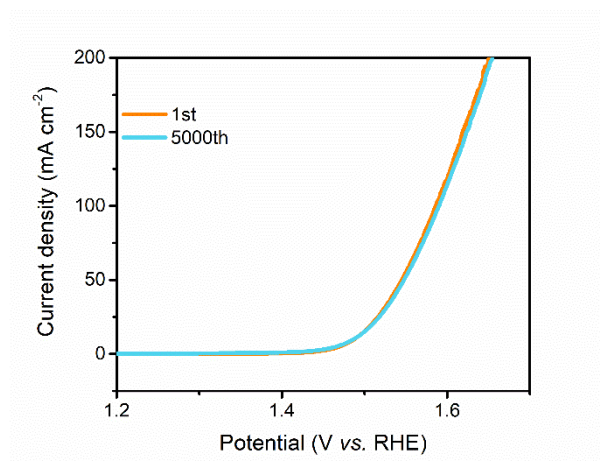
Figure S15. The polarization curves of $Co_4N@NC-700$ before and after 5000 cycles.
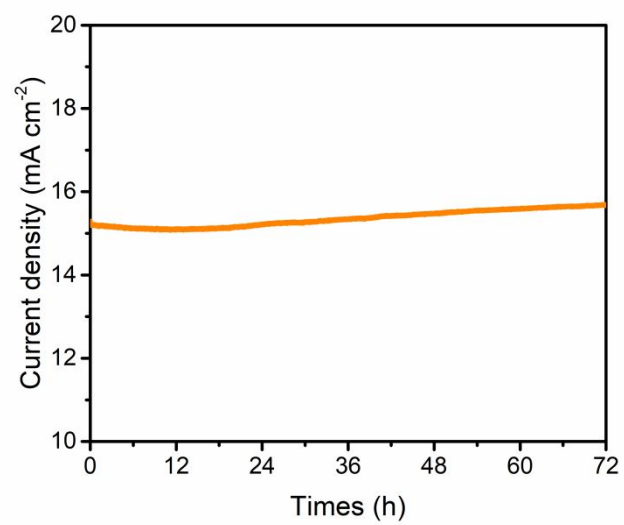
Figure S16. The i-t curves under a potential of 1.5 V vs. RHE for 72 h.
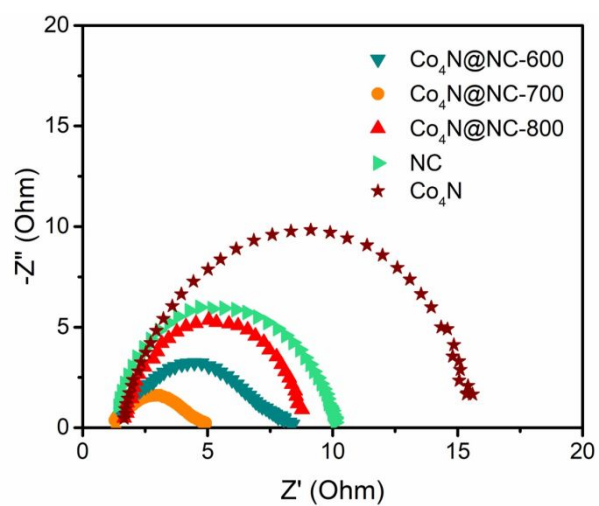
Figure S17. The Nyquist plots of Co$_4$N@NC-600, Co$_4$N@NC-700, Co$_4$N@NC-800, Co$_4$N, and NC catalysts under a potential of 1.2 V vs. RHE.

Figure S18. The CV of Co$_4$N@NC-700 (a), Co$_4$N@NC-600 (b), Co$_4$N@NC-800 (c), NC (d), and Co$_4$N (e) at a potential of 1.0-1.1 V v.s. RHE.
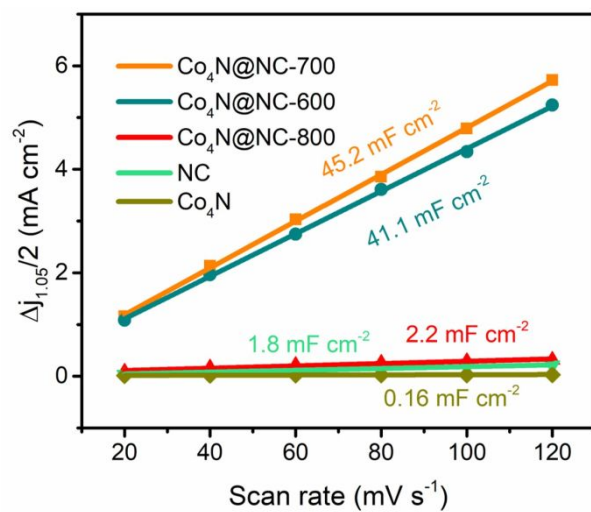
Figure S19. ECSA of $Co_4N@NC-600$, $Co_4N@NC-700$, $Co_4N@NC-800$, Co_4N, and NC catalysts.

Table S3. The water-splitting performance of $Co_4N@NC// Co_4N@NC$ electrolyzer and other previous reported state-of-art non-precious metal-based electrolyzers

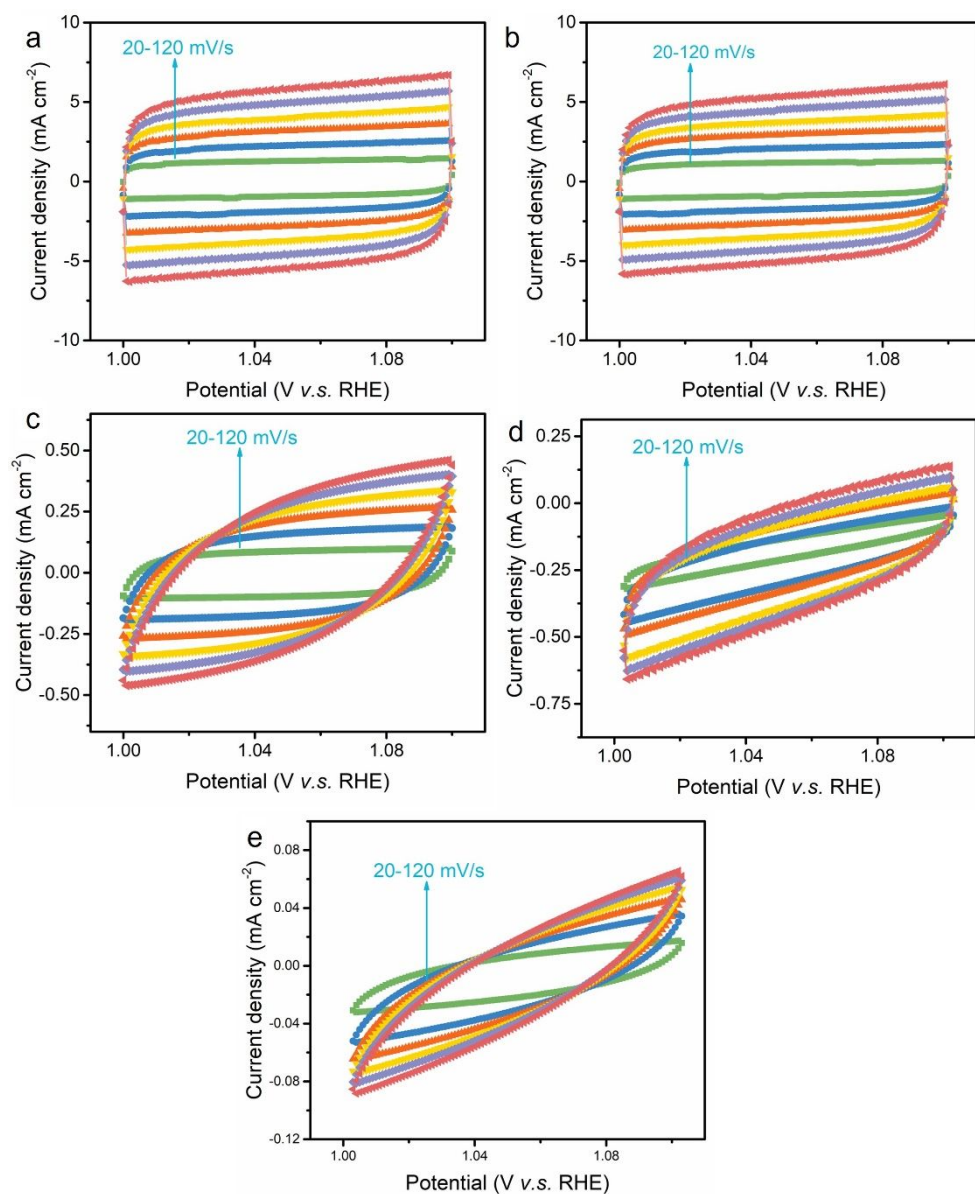| Catalysts	Mass loading (mg cm^{-2})	Media	η@10mA cm^{-2} (V)	Ref.
$Co_4N@NC$	0.285	1M KOH	1.55	This work
Ni_3FeN-NPs	0.35	1M KOH	1.58	[10]
$Co_{5.47}N@NC$	0.45	1M KOH	1.62	[13]
CoN@VON	2	1M KOH	1.64	[14]
CoN@CC	Not Given	1M KOH	1.59	[15]
FeOOH@Co4N	2	1M KOH	1.59	[16]
CoO-Co_4N	Not Given	1M PBS	1.79	[17]
$Co(OH)_2@Ni$	~7.5	1M KOH	1.64	[18]
CoP@rGO	~0.28	1M KOH	1.70	[19]
CoS_2	~1.2	1M KOH	1.67	[21]
N,F-G	2.55	1M KOH	1.91	[25]
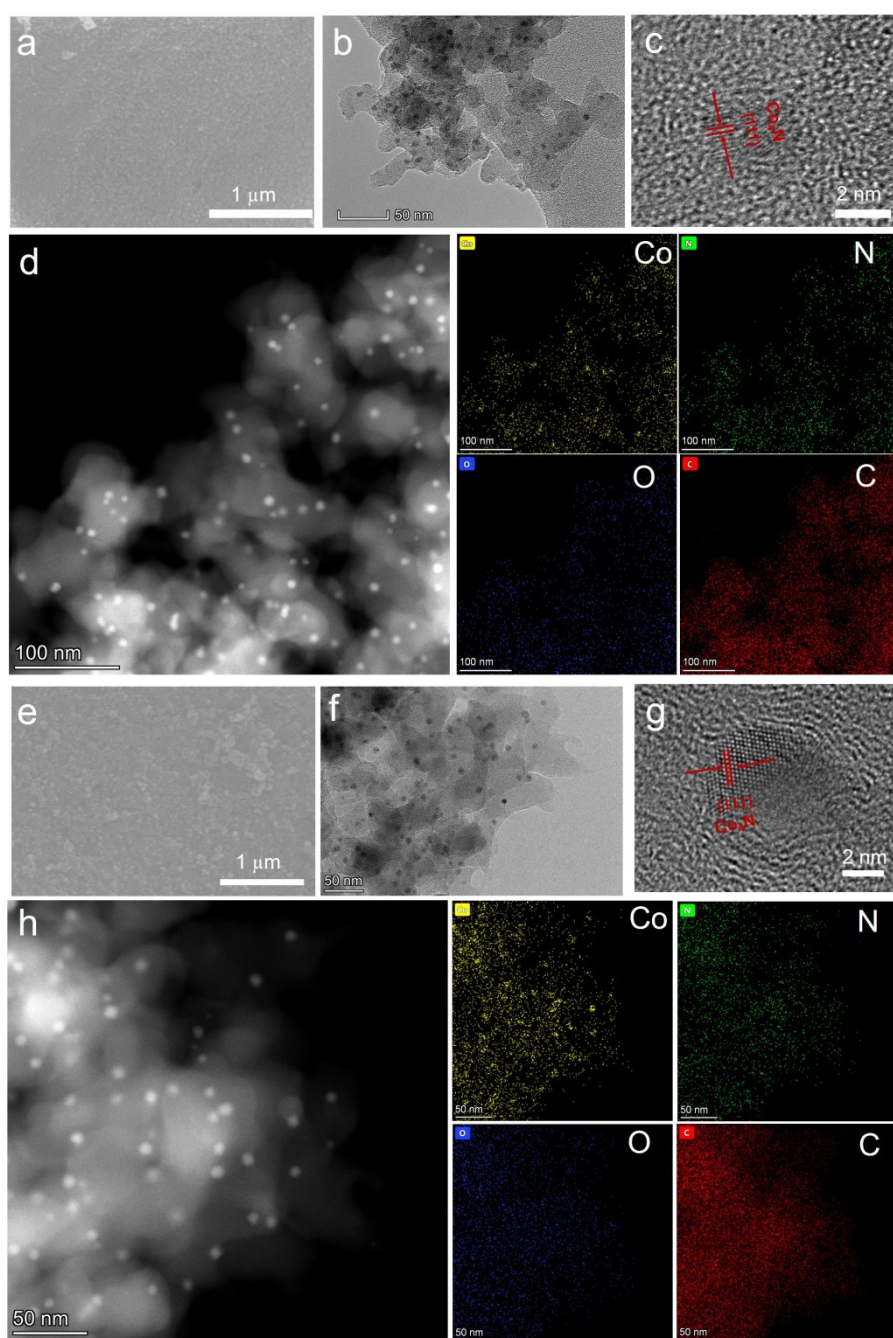
Figure S20. The morphology of Co₄N@NC cathode (a-d) and cathode (e-h) after cycling tests.
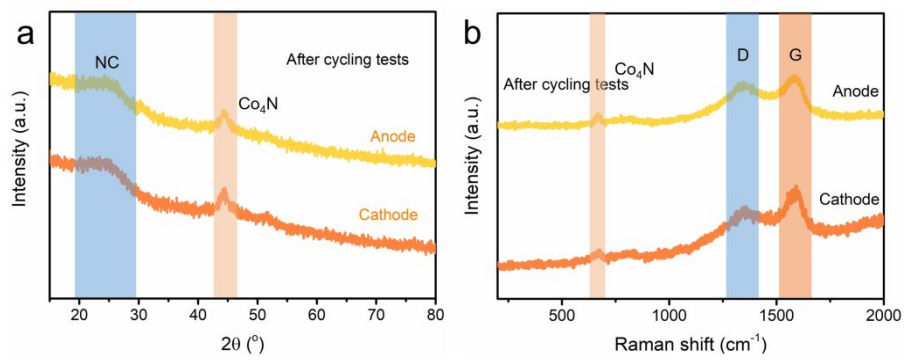
Figure S21. XRD (a) and Raman (b) spectra of Co$_4$N@NC after cycling tests.
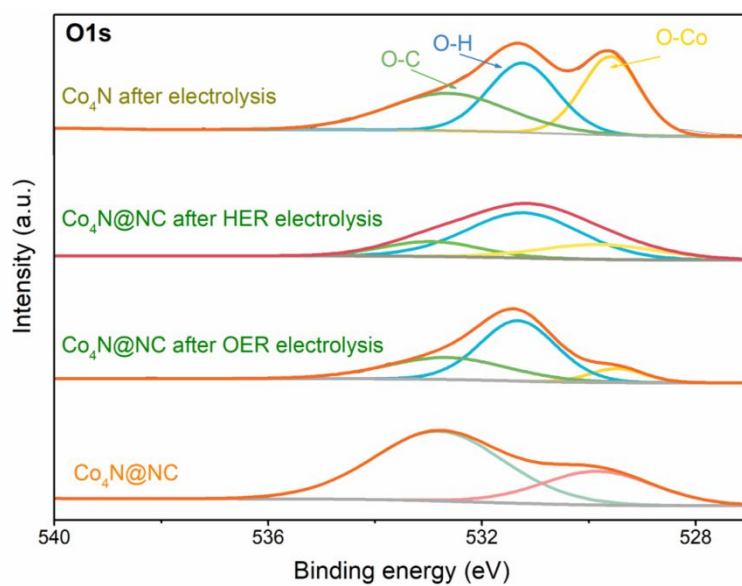
Figure S22. The O1s XPS spectra of $Co_4N@NC$ catalyst, after continuous electrocatalysis, and Co_4N after continuous electrocatalysis. The XPS spectra was directly carried out the dried catalysts that were directly taken out from the KOH solution after electrocatalysis.

Figure S23. Schematic structures of Co_4N (a) and NC (b) for DFT calculations.

REFERENCES

(1) Wu, H.-L.; Huff, L. A.; Esbenshade, J. L.; Gewirth, A. A. J. A. a. m.; interfaces, In situ EQCM study examining irreversible changes the sulfur–carbon cathode in lithium–sulfur batteries. *ACS Appl. Mater. Interfaces* **2015**, 7 (37), 20820-20828.

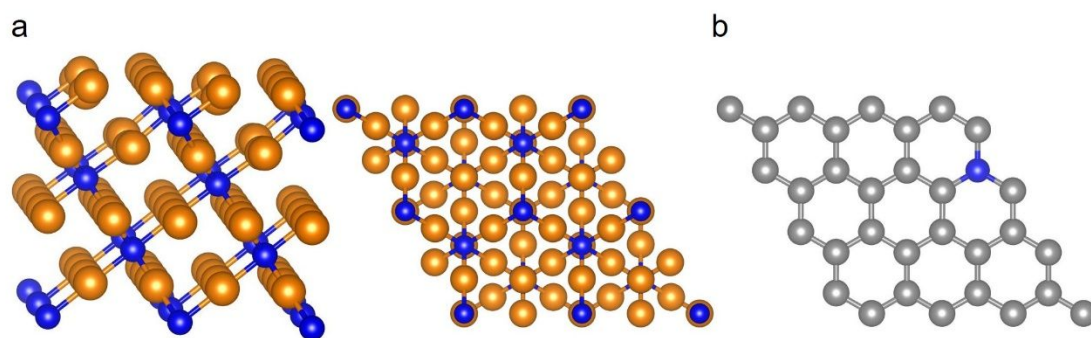(2) Tomita, K.; Noguchi, H.; Uosaki, K., Effect of Water and HF on the Distribution of Discharge Products at Li–O$_2$ Battery Cathode. A*CS Appl. Energy Mater*. **2018**, 1 (7), 3434-3442.

(3) Tiwari, J. N.; Sultan, S.; Myung, C. W.; Yoon, T.; Li, N.; Ha, M.; Harzandi, A. M.; Park, H. J.; Kim, D. Y.; Chandrasekaran, S. S.; Lee, W. G.; Vij, V.; Kang, H.; Shin, T. J.; Shin, H. S.; Lee, G.; Lee, Z.; Kim, K. S., Multicomponent electrocatalyst with ultralow Pt loading and high hydrogen evolution activity. *Nat. Energy* **2018**, 3 (9), 773-782.

(4) Giannozzi, P.; Baroni, S.; Bonini, N.; Calandra, M.; Car, R.; Cavazzoni, C.; Ceresoli, D.; Chiarotti, G. L.; Cococcioni, M.; Dabo, I.; Dal Corso, A.; de Gironcoli, S.; Fabris, S.; Fratesi, G.; Gebauer, R.; Gerstmann, U.; Gougoussis, C.; Kokalj, A.; Lazzeri, M.; Martin-Samos, L.; Marzari, N.; Mauri, F.; Mazzarello, R.; Paolini, S.; Pasquarello, A.; Paulatto, L.; Sbraccia, C.; Scandolo, S.; Sclauzero, G.; Seitsonen, A. P.; Smogunov, A.; Umari, P.; Wentzcovitch, R. M., QUANTUM ESPRESSO: a modular and open-source software project for quantum simulations of materials. *J. Phys.: Condens. Matter* **2009**, 21 (39), 395502.

(5) Blöchl, P. E., Projector augmented-wave method. *Phys. Rev. B* **1994**, 50 (24), 17953-17979.

(6) Perdew, J. P.; Burke, K.; Ernzerhof, M., Generalized Gradient Approximation Made Simple. *Phys. Rev. Lett.* **1996**, 77 (18), 3865-3868.

(7) Monkhorst, H. J.; Pack, J. D., Special points for Brillouin-zone integrations. *Phys. Rev. B* **1976**, 13 (12), 5188-5192.

(8) Bengtsson, L., Dipole correction for surface supercell calculations. *Phys. Rev. B* **1999**, 59 (19), 12301-12304.

(9) Ling, C.; Shi, L.; Ouyang, Y.; Zeng, X. C.; Wang, J., Nanosheet Supported Single-Metal Atom Bifunctional Catalyst for Overall Water Splitting. *Nano Lett*. **2017**, 17 (8), 5133-5139.

(10) Jia, X.; Zhao, Y.; Chen, G.; Shang, L.; Shi, R.; Kang, X.; Waterhouse, G. I. N.; Wu, L.-Z.; Tung, C.-H.; Zhang, T., Ni3FeN Nanoparticles Derived from Ultrathin NiFe-Layered Double Hydroxide Nanosheets: An Efficient Overall Water Splitting Electrocatalyst. *Adv. Energy Mater.* **2016**, 6 (10), 1502585.

(11) Xu, Z.; Li, W.; Yan, Y.; Wang, H.; Zhu, H.; Zhao, M.; Yan, S.; Zou, Z., In-Situ Formed Hydroxide Accelerating Water Dissociation Kinetics on Co$_3$N for Hydrogen Production in Alkaline Solution. A*CS Appl. Mater. Interfaces 2018*, 10 (26), 22102-22109.

(12) Liu, B.; Cheng, J.; Peng, H.-Q.; Chen, D.; Cui, X.; Shen, D.; Zhang, K.; Jiao, T.; Li, M.; Lee, C.-S.; Zhang, W., In situ nitridated porous nanosheet networked Co$_3$O$_4$–Co$_4$N heteronanostructures supported on hydrophilic carbon cloth for highly efficient electrochemical hydrogen evolution. *J. Mater. Chem. A 2019*, 7 (2), 775-782.

(13) Chen, Z.; Ha, Y.; Liu, Y.; Wang, H.; Yang, H.; Xu, H.; Li, Y.; Wu, R., In Situ Formation of Cobalt Nitrides/Graphitic Carbon Composites as Efficient Bifunctional Electrocatalysts for Overall Water Splitting. *ACS Appl. Mater. Interfaces 2018*, 10 (8), 7134-7144.

(14) Dutta, S.; Indra, A.; Feng, Y.; Han, H.; Song, T., Promoting electrocatalytic overall water splitting with nanohybrid of transition metal nitride-oxynitride. *Appl. Catal. B: Environ.* **2019,** 241, 521-527.

(15) Xue, Z.; Kang, J.; Guo, D.; Zhu, C.; Li, C.; Zhang, X.; Chen, Y., Self-supported cobalt nitride porous nanowire arrays as bifunctional electrocatalyst for overall water splitting. *Electrochim. Acta* **2018**, 273, 229-238.

(16) Hu, Y.; Yang, H.; Chen, J.; Xiong, T.; Balogun, M. J. T.; Tong, Y., Efficient Hydrogen Evolution Activity and Overall Water Splitting of Metallic Co_4N Nanowires through Tunable d-Orbitals with Ultrafast Incorporation of FeOOH. *ACS Appl. Mater. Interfaces* **2019**, 11 (5), 5152-5158.

(17) Li, R.-Q.; Hu, P.; Miao, M.; Li, Y.; Jiang, X.-F.; Wu, Q.; Meng, Z.; Hu, Z.; Bando, Y.; Wang, X.-B., CoO-modified Co_4N as a heterostructured electrocatalyst for highly efficient overall water splitting in neutral media. *J. Mater. Chem. A* **2018**, 6 (48), 24767-24772.

(18) Wang, Z.; Ji, S.; Liu, F.; Wang, H.; Wang, X.; Wang, Q.; Pollet, B. G.; Wang, R., Highly Efficient and Stable Catalyst Based on $Co(OH)_2$@Ni Electroplated on Cu-Metallized Cotton Textile for Water Splitting. *ACS Appl. Mater. Interfaces* **2019**, 11 (33), 29791-29798.

(19) Jiao, L.; Zhou, Y.-X.; Jiang, H.-L., Metal–organic framework-based CoP/reduced graphene oxide: high-performance bifunctional electrocatalyst for overall water splitting. *Chem. Sci.* **2016**, 7 (3), 1690-1695.

(20) Li, Y.; Yin, J.; An, L.; Lu, M.; Sun, K.; Zhao, Y.-Q.; Gao, D.; Cheng, F.; Xi, P., FeS_2/CoS_2 Interface Nanosheets as Efficient Bifunctional Electrocatalyst for Overall Water Splitting. *Small* **2018**, 14 (26), 1801070.

(21) Guan, C.; Liu, X.; Elshahawy, A. M.; Zhang, H.; Wu, H.; Pennycook, S. J.; Wang, J., Metal–organic framework derived hollow CoS_2 nanotube arrays: an efficient bifunctional electrocatalyst for overall water splitting. *Nanoscale Horiz.* **2017**, 2 (6), 342-348.

(22) Fei, H.; Dong, J.; Arellano-Jiménez, M. J.; Ye, G.; Kim, N. D.; Samuel, E. L.; Peng, Z.; Zhu, Z.; Qin, F.; Bao, J., Atomic cobalt on nitrogen-doped graphene for hydrogen generation. *Nat. Commun.* **2015**, 6, 8668.

(23) Qu, K.; Zheng, Y.; Jiao, Y.; Zhang, X.; Dai, S.; Qiao, S. Z., Polydopamine-Inspired, Dual Heteroatom-Doped Carbon Nanotubes for Highly Efficient Overall Water Splitting. *Adv. Energy Mater.* **2017**, 7 (9), 1602068.

(24) Bayatsarmadi, B.; Zheng, Y.; Tang, Y.; Jaroniec, M.; Qiao, S. Z., Significant Enhancement of Water Splitting Activity of N-Carbon Electrocatalyst by Trace Level Co Doping. *Small* **2016**, 12 (27), 3703-3711.

(25) Yue, X.; Huang, S.; Cai, J.; Jin, Y.; Shen, P. K., Heteroatoms dual doped porous graphene nanosheets as efficient bifunctional metal-free electrocatalysts for overall water-splitting. *J. Mater. Chem. A* **2017**, 5 (17), 7784-7790.

(26) Tabassum, H.; Guo, W.; Meng, W.; Mahmood, A.; Zhao, R.; Wang, Q.; Zou, R., Metal–Organic Frameworks Derived Cobalt Phosphide Architecture Encapsulated into B/N Co-Doped Graphene Nanotubes for All pH Value Electrochemical Hydrogen Evolution. *Adv. Energy Mater.* **2017**, 7 (9), 1601671.

(27) Zhu, X.; Jin, T.; Tian, C.; Lu, C.; Liu, X.; Zeng, M.; Zhuang, X.; Yang, S.; He, L.; Liu, H.; Dai, S., In Situ Coupling Strategy for the Preparation of FeCo Alloys and Co_4N Hybrid for Highly Efficient Oxygen Evolution. *Adv. Mater.* **2017**, 29 (47), 1704091.

(28) Meng, F.; Zhong, H.; Bao, D.; Yan, J.; Zhang, X., In Situ Coupling of Strung Co4N and Intertwined N-C Fibers toward Free-Standing Bifunctional Cathode for Robust, Efficient, and Flexible Zn-Air Batteries. *J. Am. Chem. Soc.* **2016**, 138 (32), 10226-31.

(29) Zhang, Y.; Ouyang, B.; Xu, J.; Jia, G.; Chen, S.; Rawat, R. S.; Fan, H. J., Rapid Synthesis of

Cobalt Nitride Nanowires: Highly Efficient and Low-Cost Catalysts for Oxygen Evolution. *Angew. Chem. Int. Ed.* **2016**, 55 (30), 8670-4.

(30) Zhong, X.; Jiang, Y.; Chen, X.; Wang, L.; Zhuang, G.; Li, X.; Wang, J.-g., Integrating cobalt phosphide and cobalt nitride-embedded nitrogen-rich nanocarbons: high-performance bifunctional electrocatalysts for oxygen reduction and evolution. *J. Mater. Chem. A* **2016**, 4 (27), 10575-10584.

(31) Huang, J.; Chen, J.; Yao, T.; He, J.; Jiang, S.; Sun, Z.; Liu, Q.; Cheng, W.; Hu, F.; Jiang, Y.; Pan, Z.; Wei, S., CoOOH Nanosheets with High Mass Activity for Water Oxidation. *Angew. Chem. Int. Ed.* **2015**, 54 (30), 8722-8727.

(32) Zhang, M.; Dai, Q.; Zheng, H.; Chen, M.; Dai, L., Novel MOF-Derived Co@N-C Bifunctional Catalysts for Highly Efficient Zn–Air Batteries and Water Splitting. *Adv. Mater.* **2018**, 30 (10), 1705431.